

Article

From SuperTIGER to TIGERISS

B. F. Rauch^{1,*†‡}, W. V. Zober^{1,†‡}, Q. Abarr^{2,†}, Y. Akaike^{3,†}, W. R. Binns^{1,†}, R. F. Borda^{4,‡}, R. G. Bose^{1,†,‡}, T. J. Brandt^{5,†}, D. L. Braun^{1,†}, J. H. Buckley^{1,†,‡}, N. W. Cannady^{4,6,7,†,‡}, S. Coutu^{8,9,‡}, R. M. Crabill^{10,†}, P. F. Dowkontt^{1,†}, M. H. Israel^{1,†}, M. Kandula^{11,‡}, J. F. Krizmanic^{6,†,‡}, A. W. Labrador^{10,†}, W. Labrador^{1,†,‡}, L. Lisalda^{1,†,‡}, J. V. Martins^{4,‡}, M. P. McPherson^{12,‡}, R. A. Mewaldt^{10,†}, J. G. Mitchell^{13,‡}, J. W. Mitchell^{6,†,‡}, S. A. I. Mognet^{8,9,‡}, R. P. Murphy^{14,†}, G. A. de Nolfo^{13,†,‡}, S. Nutter^{15,†,‡}, M. A. Olevitch^{1,†}, N. E. Osborn^{1,†,‡}, I. M. Pastrana^{1,‡}, K. Sakai^{16,†,‡}, M. Sasaki^{6,7,17,†,‡}, S. Smith^{12,‡}, H. A. Tolentino^{18,‡}, N. E. Walsh^{1,†}, J. E. Ward^{19,†}, D. Washington^{8,‡}, A. T. West^{20,†} and L. P. Williams^{21,‡}

- ¹ Department of Physics and McDonnell Center for the Space Sciences, Washington University in St. Louis, St. Louis, MO 63130, USA; wzober@wustl.edu (W.V.Z.); wrb@wustl.edu (W.R.B.); labrador.w@wustl.edu (W.L.); izabella.pastrana@wustl.edu (I.M.P.)
 - ² Department of Physics and Astronomy and The Bartol Research Institute, University of Delaware, Newark, DE 19716, USA; qabarr@udel.edu
 - ³ Waseda Research Institute for Science and Engineering, Waseda University, Shinjuku City, Tokyo 169-8050, Japan
 - ⁴ Department of Physics, University of Maryland, Baltimore County, Baltimore, MD 21250, USA; nicholas.w.cannady@nasa.gov (N.W.C.); martins@umbc.edu (J.V.M.)
 - ⁵ SRON Netherlands Institute for Space Research, 2333 CA Leiden, The Netherlands; t.j.brandt@sron.nl
 - ⁶ NASA Goddard Space Flight Center, Astrophysics Science Division, Greenbelt, MD 20771, USA; john.f.krizmanic@nasa.gov (J.F.K.)
 - ⁷ Center for Research and Exploration in Space Sciences and Technology II, Greenbelt, MD 20771, USA
 - ⁸ Department of Physics, Pennsylvania State University, State College, PA 16801, USA; sxc56@psu.edu (S.C.)
 - ⁹ Institute for Gravitation and the Cosmos, Pennsylvania State University, State College, PA 16801, USA
 - ¹⁰ Space Astrophysics and Space Radiation Laboratory, California Institute of Technology, Pasadena, CA 91125, USA
 - ¹¹ Space Coast Science, Engineering & Operations Group, KBR, Titusville, FL 32780, USA
 - ¹² Department of Mechanical Engineering, Howard University, Washington, DC 20059, USA
 - ¹³ NASA Goddard Space Flight Center, Heliophysics Science Division, Greenbelt, MD 20771, USA; john.g.mitchell@nasa.gov (J.G.M.); georgia.a.denolfo@nasa.gov (G.A.d.N.)
 - ¹⁴ National Academies of Sciences, Engineering, and Medicine, Washington, DC 20001, USA
 - ¹⁵ Department of Physics and Geology, Northern Kentucky University, Highland Heights, KY 41099, USA
 - ¹⁶ Enrico Fermi Institute, The University of Chicago, Chicago, IL 60637, USA; kenichisakai@uchicago.edu
 - ¹⁷ Department of Astronomy, University of Maryland, College Park, MD 20742, USA
 - ¹⁸ Department of Electrical Engineering and Computer Science, Howard University, Washington, DC 20059, USA; harrellangelo.tolen@bison.howard.edu
 - ¹⁹ Spire Global, L-2763 Luxembourg-Ville, Luxembourg; john.ward@spire.com
 - ²⁰ Department of Astronomy and Steward Observatory, University of Arizona, Tucson, AZ 85719, USA
 - ²¹ Electro-Mechanical & Systems Engineering Group, KBR, Greenbelt, MD 20771, USA; liam.williams@us.kbr.com
- * Correspondence: brauch@physics.wustl.edu; Tel.: +1-314-935-6354
† These authors are SuperTIGER Collaborators.
‡ These authors are TIGERISS Collaborators.



Citation: Rauch, B.F.; Zober, W.V.; Abarr, Q.; Akaike, Y.; Binns, W.R.; Borda, R.F.; Bose, R.G.; Brandt, T.J.; Braun, D.L.; Buckley, J.H.; et al. From SuperTIGER to TIGERISS. *Instruments* **2024**, *8*, 4. <https://doi.org/10.3390/instruments8010004>

Academic Editors: Matteo Duranti, Valerio Vagelli and Antonio Ereditato

Received: 16 October 2023
Revised: 21 November 2023
Accepted: 28 December 2023
Published: 11 January 2024



Copyright: © 2024 by the authors. Licensee MDPI, Basel, Switzerland. This article is an open access article distributed under the terms and conditions of the Creative Commons Attribution (CC BY) license (<https://creativecommons.org/licenses/by/4.0/>).

Abstract: The Trans-Iron Galactic Element Recorder (TIGER) family of instruments is optimized to measure the relative abundances of the rare, ultra-heavy galactic cosmic rays (UHGRs) with atomic number (Z) $Z \geq 30$. Observing the UHGRs places a premium on exposure that the balloon-borne SuperTIGER achieved with a large area detector (5.6 m^2) and two Antarctic flights totaling 87 days, while the smaller ($\sim 1 \text{ m}^2$) TIGER for the International Space Station (TIGERISS) aims to achieve this with a longer observation time from one to several years. SuperTIGER uses a combination of scintillator and Cherenkov detectors to determine charge and energy. TIGERISS will use silicon strip detectors (SSDs) instead of scintillators, with improved charge resolution, signal linearity, and dynamic range. Extended single-element resolution UHGCR measurements through ^{82}Pb will cover elements produced in s-process and r-process neutron capture nucleosynthesis, adding to the multi-

messenger effort to determine the relative contributions of supernovae (SNe) and Neutron Star Merger (NSM) events to the r-process nucleosynthesis product content of the galaxy.

Keywords: galactic cosmic rays; r-process; s-process; cosmic ray detectors; cosmic ray sources; high-altitude balloons; International Space Station

1. Introduction

Ultra-heavy galactic cosmic rays (UHGCRs) are the very rare nuclei above ^{28}Ni produced in neutron capture nucleosynthesis, making them more than three orders of magnitude less abundant than those produced in stellar fusion. Measuring the UHGCRs requires the greatest possible detector exposure, which is proportional to detector area multiplied by observation time. The Super Trans-Iron Galactic Element Recorder (SuperTIGER) stratospheric balloon-borne instrument has made the best single-element resolution UHGCR measurements to date through ^{56}Ba [1–4] with a large 5.6 m^2 detector on a record-breaking 55-day flight. The Trans-Iron Galactic Element Recorder for the International Space Station (TIGERISS) will improve upon these measurements and extend them through ^{82}Pb [5,6], achieving comparable exposure in one year of observations following its planned 2026 launch with a $\sim 1\text{ m}^2$ detector area. These measurements of the UHGCRs can address questions about the grand cycle of matter in the galaxy, depicted in Figure 1, in which material from galactic cosmic ray (GCR) sources (GCRSs) is injected into the accelerator. In a picture that has been pieced together from cosmic ray elemental and isotopic composition and energy spectra measurements, the GCRs then help energize galactic magnetic fields through their electric currents and feed back into the process of new star formation, leading to more GCRs. UHGCR measurements can provide the relative abundances of r- and s-process neutron capture elements in the GCRSs as well provide clues into how this material is accelerated to cosmic ray energies.

GCR measurements, including UHGCR abundances through ^{40}Zr by TIGER and SuperTIGER, have implied a GCRS drawn primarily from older interstellar media (ISM) with fresh nucleosynthetic products of younger stars mixed in and acceleration by shock waves from stellar deaths. Supernovae (SNe) were long thought to be responsible for cosmic ray acceleration, and the r-process neutron capture nucleosynthesis of the heavier elements in the cycle is shown in Figure 1; however, recent evidence suggests that binary neutron star mergers (BNSMs) play a major role in r-process synthesis and may contribute to cosmic ray acceleration. Multi-messenger follow-up observations of a kilonovae identified in gravitational waves [7] provided broader electromagnetic spectral observations [8] that gave strong evidence for BNSM r-process nucleosynthesis of the heaviest elements. Extended SuperTIGER measurements providing the first single-element resolution UHGCR measurements through ^{56}Ba show that something is missing from the GCRS model, supported by measurements through ^{40}Zr . Superior UHGCR measurements by TIGERISS through ^{82}Pb with unprecedented resolution will address important scientific questions about GCRSs and the cosmic ray accelerator, which are discussed in more detail in [9].

the TIGER Long-Duration Balloon (LDB) payload that flew twice from Antarctica, first for 32 days from 21 December 2001 to 21 January 2002 [23,24] and again for 18 days from 17 December 2003 to 4 January 2004 [25,26]. TIGER LDB was in turn based on the original TIGER instrument that flew from Lynn Lake, Manitoba, Canada for 2.75 h on 26 August 1995 [27] and Fort Sumner, NM for 23.25 h on 25 September 1997 [28], demonstrating the instrument concept [29]. SuperTIGER uses the same two fundamental charge identification techniques demonstrated in TIGER: dE/dx vs. Cherenkov and acrylic Cherenkov vs. silica aerogel Cherenkov.

2.1. Instrument Design

Figure 2a shows a technical model of the full SuperTIGER-2.1 (2017–2018)/SuperTIGER-2.2 (2018–2019) payload comprising two instrument modules. SuperTIGER-2.3 had a 180-cell solar panel array instead of the pictured 160-cell array to support the four piggyback instruments it carried: the Advanced Particle–astrophysics Telescope (APT) prototype APTlite [30,31] and Balloon Air Sampler (BAS) [32] in addition to the Exposing Microorganisms in the Stratosphere (E-MIST) [33] and Polar Mesospheric Cloud Turbulence (PMC-Turbo) [34] pictured. An expanded view of an instrument module is shown in Figure 2b, with each module being a stack of seven detectors. Three large-area compact wavelength-shifter bar readout scintillator detectors (S1, S2, and S3) measure light production dependent on ionization energy losses ($dL/dx \propto dE/dx \propto Z^2$) and contribute to charge (Z) measurement, identification of interacting particles, and the instrument trigger. Top (H1) and bottom (H2) scintillating fiber hodoscopes provide trajectory determination for path length and areal response corrections. At the middle of the stack are two Cherenkov detectors that measure light production as a function of Z and velocity ($\beta = v/c$). Above is a silica aerogel detector (C0), with three quarters of the radiators having an index of refraction (n) $n = 1.043$ ($KE \gtrsim 2.5$ GeV/amu) and one quarter $n = 1.025$ ($KE \gtrsim 3.3$ GeV/amu); below is an acrylic detector (C1) with $n = 1.49$ ($KE \gtrsim 0.3$ GeV/amu). The combined effective geometry factor of the SuperTIGER modules after accounting for interactions is 2.9 m²sr, which is 7.2 times that of the preceding TIGER LDB instrument [35].

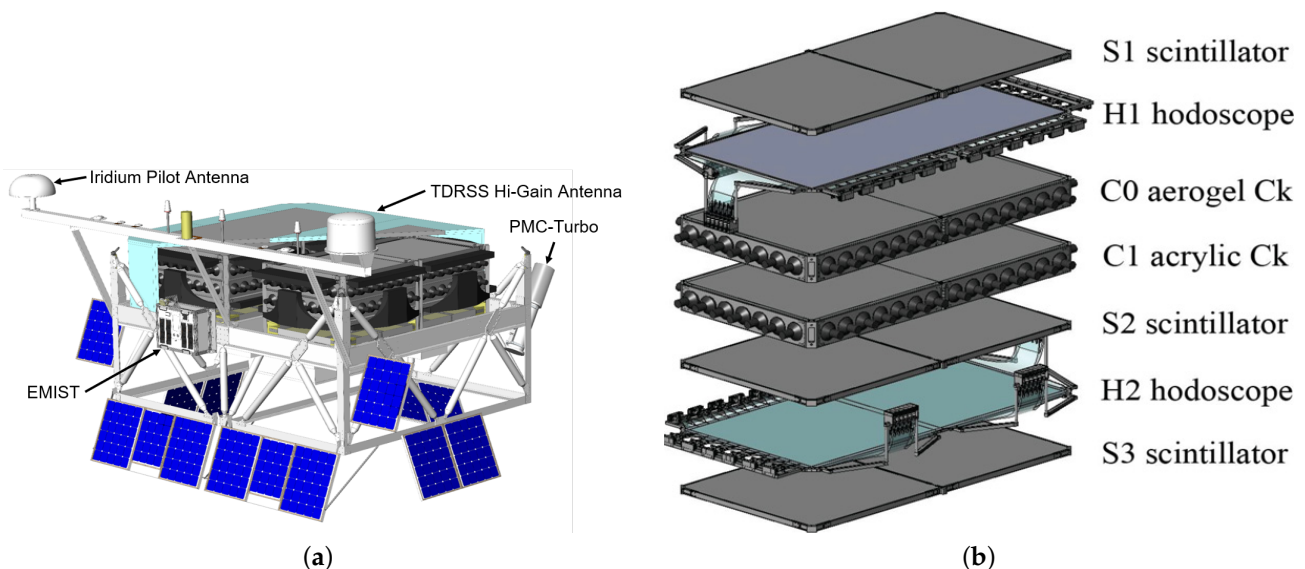


Figure 2. (a) Technical model of SuperTIGER-2.1/2.2. (b) Expanded view of a SuperTIGER module.

2.2. UHGCR Science

Figure 3a shows single-element resolution GCR abundance measurements at ~ 2 GeV/amu through ^{56}Ba [1,36–38] compared with Solar System (SS) abundances [39] through ^{82}Pb , both normalized to $^{14}\text{Si} = 1$. The differences between GCR and SS abundances for

the more abundant elements below ${}_{26}\text{Fe}$ are understood to arise largely from spallation in GCR propagation from the source, a process that increases less abundant primary element abundances through erosion of more abundant ones. The GCR composition, and particularly that of the UHGCR elements not produced in stellar fusion, provides clues about the GCRS reservoirs and the acceleration mechanism.

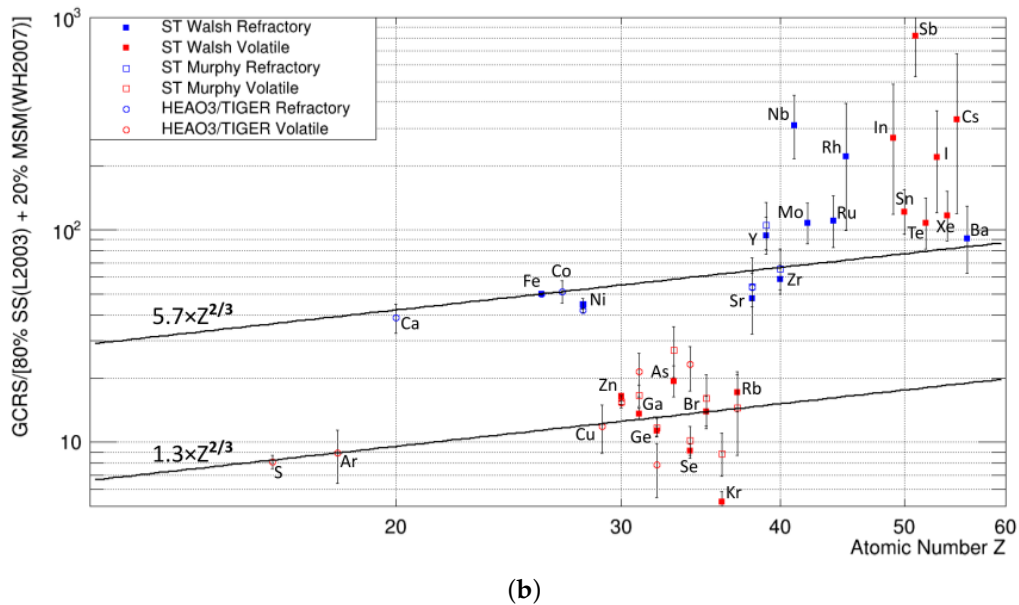
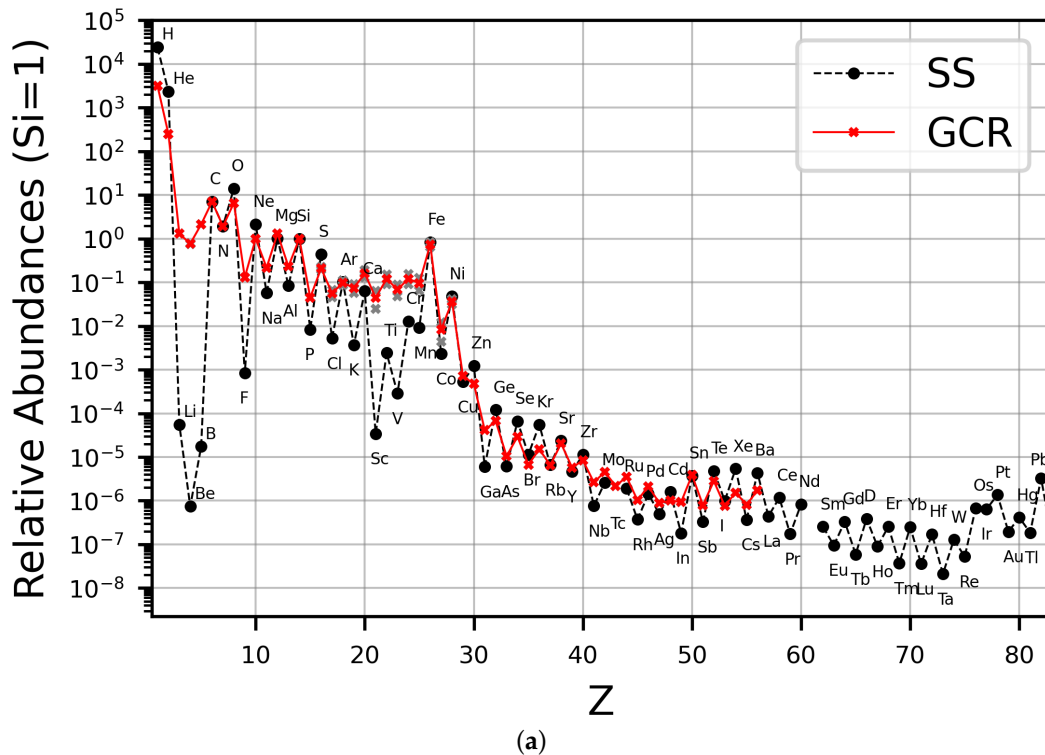


Figure 3. (a) SS [39] (dashed black line) and GCR at ~ 2 GeV/amu (solid red line) relative abundances normalized to ${}_{14}\text{Si}$. GCR data sourced for $1 \leq Z \leq 2$ from [36], $Z = 3$ from [37], $4 \leq Z \leq 28$ from [38], and $16 \leq Z \leq 56$ from [1]. Gray dots depict overlapping measurements from [1,38]. (b) GCR measurements corrected for galactic propagation back to the source relative to a GCRS model of 80% SS [39] and 20% MSM [40] versus atomic number. Refractory elements (blue) and volatile elements (red). HEAO-3-C2 ($Z \leq 28$) [38] and SuperTIGER ($Z \geq 26$) [2–4,20] through ${}_{56}\text{Ba}$ showing that the existing model is insufficient for elements above ${}_{40}\text{Zn}$.

TIGER made the first UHGCR measurements with single-element resolution through ^{40}Zr [25,26], which supported a model of GCR origins with a major component from OB associations. In this model, the GCRS is composed of $\sim 80\%$ ISM represented by SS material [39] and $\sim 20\%$ massive star material (MSM) from OB associations, including stellar winds and SN ejecta [40]. Figure 3b shows the ratio of the GCR measurements corrected for galactic propagation to the GCRS model abundances as a function of Z , with refractory elements more likely to condense onto dust grains in blue and more volatile ones in red. GCR measurements through ^{40}Zr fall around refractory and volatile lines, with the refractory elements being ~ 4.4 times more abundant. The $Z^{2/3}$ slope is proportional to the nuclear cross section, which supports an acceleration model with preferential injection of elements that sputter off of superthermal dust grains [41]. SuperTIGER measurements through ^{40}Zr [19,20] with greater statistics and improved resolution agreed with the TIGER results, but further SuperTIGER analysis pushing the UHGCR measurement through ^{56}Ba [1–4] shows that the model breaks down above ^{40}Zr . This hints at a potential new GCRS component, and TIGERISS will make measurements through ^{82}Pb with superior charge reconstruction and resolution to search for new source signatures.

2.3. Future Prospects

SuperTIGER is mostly still on the high plateau in East Antarctica ($71^\circ 7.53' \text{ S}$, $158^\circ 35.10' \text{ E}$, 6629 feet), with only a high-priority item recovery on January 21, 2020 and a data recovery on 6 November 2021. Full recovery of the payload has been delayed by the global COVID-19 pandemic, and it is now almost entirely drifted over. Recovery was initially planned for the 2022–2023 Antarctic season before being deferred to the 2023–2024 season due to limited support resource availability. With the uncertain future disposition of the payload and current backlog of Antarctic flight requests, SuperTIGER has no plans for future flights. Fortunately for the franchise, extended UHGCR analysis from the first record-breaking 55-day SuperTIGER flight hinting at new science supported a successful proposal for its successor instrument.

3. TIGERISS

TIGERISS is a UHGCR detector selected in the second round of the NASA Astrophysics Pioneers Program being developed for launch to the International Space Station (ISS) in 2026. This experiment will carry forward the UHGCR science of TIGER [26] and SuperTIGER [35] and seek an explanation for GCRS model-breaking SuperTIGER results. The TIGERISS collaboration, like the instrument, has also evolved from SuperTIGER, building on the core of WUSTL and NASA GSFC and later on UMBC and NKU additions with Pennsylvania State University (PSU) and Howard University.

TIGERISS will, in one year, measure the UHGCR abundances through ^{56}Ba with comparable statistics to SuperTIGER, while having the extended dynamic range for the first preliminary single-element charge-resolution measurements through ^{82}Pb by an active detector. Extended operations would allow TIGERISS to make more significant UHGCR measurements that will cover a wider range of elements produced in s-process and r-process neutron capture nucleosynthesis, adding to the multi-messenger effort to determine the relative contributions of SNe and Neutron Star Merger (NSM) events to r-process nucleosynthesis.

3.1. Instrument Concept

TIGERISS will use the same fundamental charge identification techniques used by TIGER/SuperTIGER: dE/dx vs. Cherenkov and acrylic Cherenkov vs. silica aerogel Cherenkov, as well as multiple dE/dx , but with improved detectors. Figure 4a gives an expanded view of the TIGERISS instrument stack, with pairs of orthogonal silicon strip detector (SSD) layers above and below the aerogel ($n = 1.05$, $\beta \geq 0.95$, $\text{KE} \gtrsim 2.12 \text{ GeV/amu}$) and acrylic ($n = 1.49$, $\beta \geq 0.67$, $\text{KE} \gtrsim 325 \text{ MeV/amu}$) Cherenkov light-collection boxes. Figure 4b shows an expanded view of an SSD layer, which will provide both dE/dx

measurements ($\propto Z^2$) and trajectory determination in place of the large-area compact wavelength-shifter bar readout scintillator detectors (dL/dx) and scintillating optical fiber hodoscopes (trajectory) used in the balloon-borne instruments. The more compact readout allowed by the SSDs and silicon photomultiplier (SiPM) modules TIGERISS will use on the Cherenkov detectors instead of photomultiplier tubes (PMTs) lets us build the largest possible instrument within the allowed payload envelope. An expanded view of a TIGERISS Cherenkov detector in Figure 4c shows that the Cherenkov-light radiators, in this case acrylic, will be at the top of the detector boxes to improve light collection over the bottom placement used in the balloon-borne instruments.

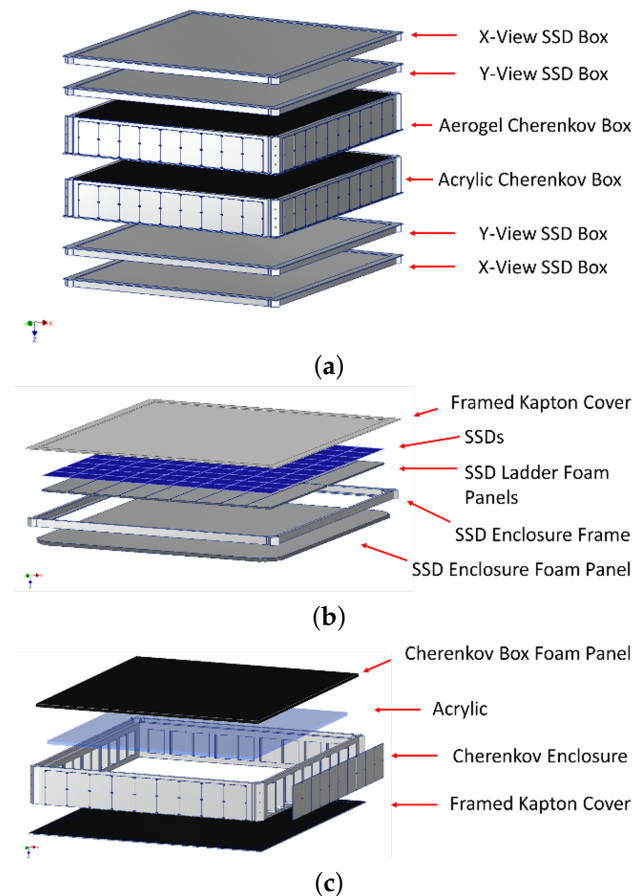


Figure 4. (a) Expanded view of the standard TIGERISS payload technical model. (b) SSD expanded view. (c) Acrylic Cherenkov detector expanded view.

3.2. Payload Model Development

There are similarities and major differences in the design requirements for balloon and space payloads. SuperTIGER was designed to operate in the very low atmospheric pressure at stratospheric altitudes, as well as to deal with major shocks in excess of 10 g experienced when the parachute opens following termination and on landing. TIGERISS will need to operate in hard vacuum, will experience shocks during launch, and will undergo acoustic and vibration loads that SuperTIGER did not. Analysis of TIGERISS detector component and payload models for launch environment conditions will be followed by some component model tests to address specific Technology Readiness Level (TRL) concerns, and ultimately by the full payload being put through thermal-vacuum, acoustic, and vibration tests.

All TIGERISS systems must meet TRL standards for launch and the ISS environment that exceed those of balloon payloads, and systems that are changed from SuperTIGER particularly benefit from heritage with other instruments. Silicon detectors have been used on many space missions, including ACE-CRIS [42], Light Imager for Gamma-ray

Astrophysics (AGILE) [43], Alpha Magnetic Spectrometer (AMS-02) [44], Energetic Particles: Acceleration, Composition, and Transport investigation (EPACT) on the Global Geospace Science (GGS) Wind satellite [45], Fermi-Large Area Telescope (Fermi-LAT) [46], Payload for Antimatter Matter Exploration and Light-nuclei Astrophysics (PAMELA) [47], Parker Solar Probe [48], and the Solar Terrestrial Relations Observatory (STEREO) [49]. TIGERISS will use daisy-chained detector ladders that are particularly similar to those used in AMS-02 [44] and Fermi-LAT [46]. TIGERISS SiPM components are similar to those used on two CubeSat missions, Ionospheric Neutron Content Analyzer (INCA) [50] and BurstCube [51], using carrier and summing electronics for SiPM arrays developed for APT [52] and the Antarctic Demonstrator for the Advanced Particle-Astrophysics Telescope (ADAPT), Solar Neutron TRACKing (SONTRAC) [53], and the High-Energy Light Isotope eXperiment (HELIX) [54]. TIGERISS will use a data acquisition (DAQ) system based on field-programmable gate arrays (FPGAs) based on that flown on the HyperAngular Rainbow Polarimeter (HARP) CubeSat [55] and in development for the HARP2 instrument on the Plankton, Aerosol, Clouds, ocean Ecosystem (PACE) mission [56].

The Japan Aerospace Exploration Agency (JAXA) Japanese Experiment Module (JEM) “Kibo” Exposed Facility Unit 10 (EFU10) location originally proposed for TIGERISS is now expected to be occupied by ECOSystem Spaceborne Thermal Radiometer Experiment on Space Station (ECOSTRESS) [57] when TIGERISS is planned to launch to the ISS in June 2026, and we were directed to investigate all possible ISS external payload accommodation sites. Until August 13, 2023, these included JEM-EFU6 and JEM-EFU7, as well as the European Space Agency (ESA) Columbus Laboratory external payload Starboard Overhead X-Direction (SOX) location. We have been notified by the ISS Program Office that the Global Ecosystem Dynamics Investigation (GEDI) payload [58] is planned until the end of the ISS for JEM-EFU6. None of the zenith-facing NASA Expedite the Processing of Experiments to the Space Station (ExPRESS) Logistics Carrier (ELC) locations are expected to be available for TIGERISS. Detailed payload technical models for the SOX (Figure 5a) and JEM-EF (Figure 5b) locations are under development, including a standard JEM-EF model configuration and one 0.2 m wider for JEM-EFU7 that would require a JAXA waiver. Table 1 gives instrument dimensions and geometry factors for these models and the one used in the proposal.

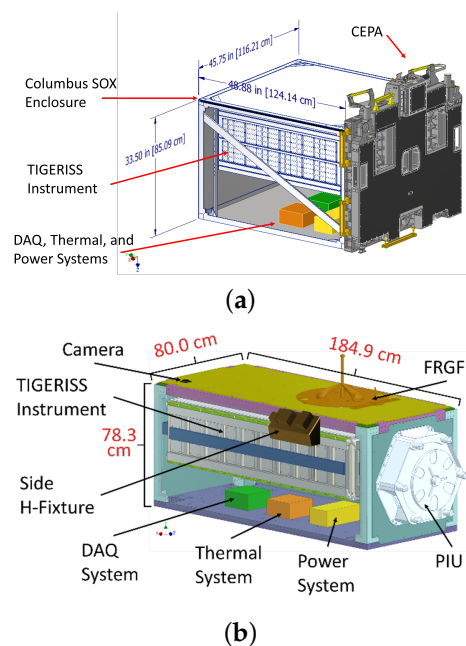


Figure 5. (a) Columbus SOX TIGERISS payload technical model. (b) JEM-EF standard TIGERISS payload technical model.

Table 1. TIGERISS instrument dimensions and geometry factors.

ISS Attachment	Length	Width	Height	Area	Geometry Factor
JEM-EF proposal	1.67 m	0.67 m	0.40 m	1.12 m ²	1.66 m ² sr
Columbus SOX	1.00 m	0.90 m	0.42 m	0.90 m ²	1.28 m ² sr
JEM-EF standard	1.50 m	0.60 m <td 0.42 m	0.90 m ²	1.19 m ² sr	
JEM-EF wide	1.50 m	0.80 m	0.42 m	1.20 m ²	1.83 m ² sr

3.3. Thermal Analysis

The thermal environment on the ISS is significantly different than for stratospheric-balloon payloads. SuperTIGER was able to maintain all detector and electronics systems within acceptable temperature ranges with the use of insulation and thermostat-triggered heaters on the most sensitive electronics. It also used a rotator system to point the solar array toward the sun, which introduced a fixed thermal gradient from the hot to cold sides. The widely varying solar illumination and Earth albedo conditions TIGERISS will experience require both active heating and radiator heat dissipation.

TIGERISS thermal analysis efforts have been carrying both Columbus SOX and JEM-EF payload configurations. With the elimination of the JEM-EFU6 location with an active coolant loop, just the JEM-EFU7 and Columbus SOX locations remain, which only have passive thermal control and heaters. Integrated ISS thermal modeling for a range of orbital conditions has been performed, with a focus on hot and cold cases to assess radiator sizing and heater power budget needs. Figure 6a shows the TIGERISS SOX mechanical model, including thermal radiators mounted to Columbus Laboratory, and Figure 6b shows the payload as part of the Integrated ISS thermal model. The launch and orbital cases where limited power is available for survival heaters, as well as the up to seven hours without power during installation, are also being studied. Current modeling finds that expected thermal conditions will be within TIGERISS component tolerances and that heater power and radiator space needs are safely within limits. As with SuperTIGER, TIGERISS will correct for time-varying detector gain responses from changing temperatures by normalizing detector signals using ²⁶Fe and/or other of the more abundant cosmic ray nuclei species.

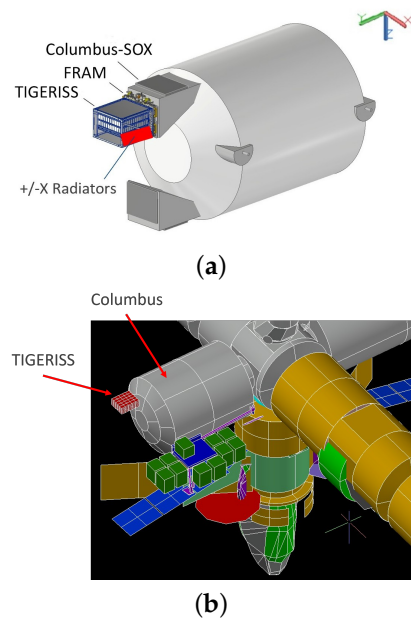


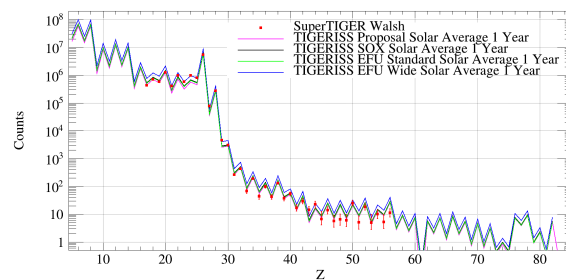
Figure 6. (a) Columbus SOX TIGERISS payload technical model showing radiators. (b) Columbus SOX TIGERISS payload thermal model.

3.4. Predicted TIGERISS Measurements

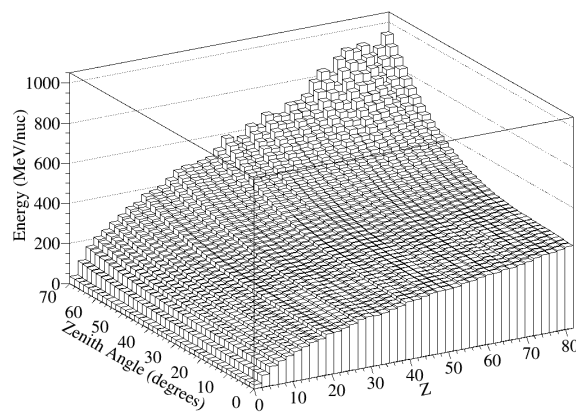
Predictions for TIGERISS event statistics incorporate cosmic ray spectra and corrections for geomagnetic screening, instrument thresholds, and interactions in the instrument based on a method originally developed for the CALET [59]. For elements from ${}^5\text{B}$ to ${}^{32}\text{Ge}$, energy spectra have been measured by the ACE-CRIS at the L1 Lagrange Point [60]. For UHGCR elements for which energy spectra have not been measured, the ${}^{26}\text{Fe}$ spectrum is scaled using SuperTIGER relative abundances for elements through ${}^{40}\text{Zr}$ [20]. The predictions between ${}^{40}\text{Zr}$ and ${}^{60}\text{Nd}$ are based on the assumed 20% odd/80% even splitting of charge pairs measured by HEAO-3-HNE [14], which agree reasonably with the SuperTIGER measurements [2], and abundances of elements in charge groups above ${}^{60}\text{Nd}$ are scaled by SS abundances [39]. The level of solar modulation does not have a strong impact on the TIGERISS UHGCR measurements due to significant geomagnetic screening in the ISS 51.6° inclination orbit.

3.4.1. Statistics from One Year

TIGERISS GCR statistics for ISS observations have been generated for the new instrument models under study [6]. Figure 7a gives predicted one-year TIGERISS measurements for the proposed JEM-EF model (pink), Columbus SOX model (black), current JEM-EF standard model (green), and JEM-EF wide model (blue) configurations [6] compared with those from the first SuperTIGER flight (red) [1–4]. The expected TIGERISS one-year statistics are comparable to or better than those for SuperTIGER where their sensitive ranges overlap.



(a)



(b)

Figure 7. (a) Predicted abundances measured by TIGERISS after one year of operation [6] compared to those measured by SuperTIGER over its first 55-day long-duration balloon flight [1–4]. (b) Incident threshold energy (MeV/amu) required to trigger TIGERISS as a function of Z and zenith angle (θ) [6].

Table 1 shows that only the wide JEM-EF model has a larger geometry factor than the proposed TIGERISS instrument, but Figure 7a shows that all of the new models are expected to outperform it. Addressing subsystem interface requirements to constrain the

mechanical model design envelopes for needed electronics, cabling, and thermal systems resulted in the standard JEM-EF instrument configuration in the proposal being downsized by 17 cm in length and 7 cm in width, as shown in Table 1. The superior performance of the newer models is due to the calculations used in the proposal only accepting events above a conservative energy threshold [61]. The current calculations [6] use the angle-dependent threshold energies derived for each element from Geant4 simulations, shown in Figure 7b. These results show that TIGERISS instrument models with higher confidence of design after the first year of development can deliver the scientific results promised in the proposal.

3.4.2. Statistics from Extended Observations

The ISS is now planned to operate through 2030, and if TIGERISS delivers as planned, its operations may be extended through the end of the ISS. Expected TIGERISS statistics from three years of observations under average solar modulation are shown in Figure 8 for the same payload configurations shown in Figure 7a. The increased UHGCR statistics from extended TIGERISS operations will resolve most even and many odd-Z elements, including the important ^{76}Os , ^{78}Pt , and ^{82}Pb abundances, with greater statistical significance.

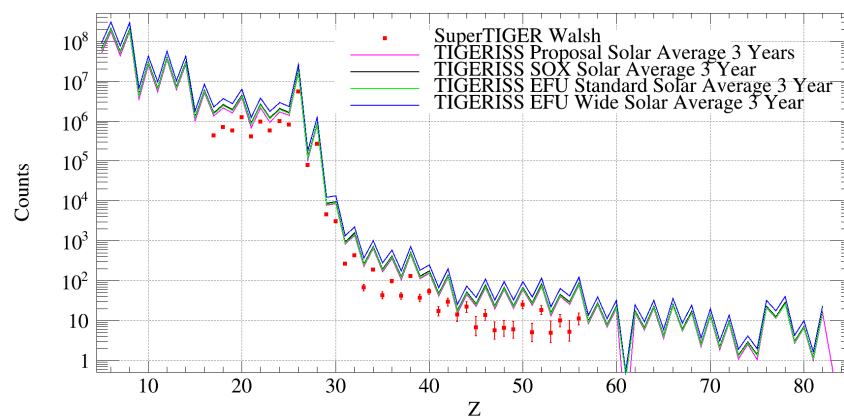


Figure 8. Predicted abundances measured by TIGERISS after three years of operation [5,6], compared to those measured by SuperTIGER over its first 55-day long-duration balloon flight [1–4].

4. Conclusions

The stratospheric balloon-borne SuperTIGER instrument has made the best single-element resolution UHGCR measurements to date through ^{56}Ba ; the TIGERISS instrument, with a planned 2026 launch, will extend these to ^{82}Pb with superior resolution. Switching from scintillator detectors to SSDs for position and charge measurement will provide better charge resolution and linearity for TIGERISS, allowing it to measure all GCRs from 5B to ^{82}Pb with a single instrument. SuperTIGER results have shown that there is something missing from the OB Association GCRS model, and TIGERISS will probe for other GCRS signatures and test GCR acceleration models through ^{82}Pb . With the one year of observations possible under the five-year performance period of the Astrophysics Pioneers Program, TIGERISS will test SuperTIGER measurements with different systematics. If these measurements agree, they will effectively double the UHGCR single-element resolution statistics through ^{56}Ba . Regardless, TIGERISS will provide the first single-element resolution UHGCR measurements from ^{56}Ba to ^{82}Pb , measuring further up the periodic table the relative contributions of r- and s-process neutron capture sources to the GCRs.

Author Contributions: All authors with [†] supported SuperTIGER, and all authors with [‡] have supported the conceptualization and design of TIGERISS. Conceptualization, L.P.W., J.V.M., B.F.R., W.V.Z., W.R.B., R.F.B., R.G.B., T.J.B., D.L.B., J.H.B., N.W.C., S.C., P.F.D., M.H.I., J.F.K., L.L., M.P.M., R.A.M., J.G.M., J.W.M., S.A.I.M., G.A.d.N., S.N., N.E.O., I.M.P., K.S., M.S., S.S., H.A.T., N.E.W., D.W.; methodology, L.P.W., B.F.R., W.V.Z., W.R.B., S.C., M.H.I., M.K., J.F.K., A.W.L., W.L., M.P.M., J.G.M.,

J.W.M., S.A.I.M., R.P.M., S.N., N.E.O., I.M.P., K.S., M.S., S.S., H.A.T., N.E.W., D.W.; software, L.P.W., J.V.M., B.F.R., W.V.Z., Y.A., R.F.B., R.G.B., N.W.C., J.F.K., A.W.L., W.L., S.A.I.M., R.P.M., S.N., M.A.O., N.E.O., I.M.P., K.S., M.S., H.A.T., N.E.W., D.W.; validation, L.P.W., J.V.M., R.M.C., B.F.R., W.V.Z., Q.A., R.F.B., R.G.B., D.L.B., P.F.D., M.K., W.L., L.L., M.P.M., J.G.M., S.A.I.M., R.P.M., S.N., M.A.O., N.E.O., I.M.P., M.S., S.S., H.A.T., N.E.W., D.W., A.T.W.; formal analysis, B.F.R., W.V.Z., N.W.C., S.C., M.K., J.F.K., A.W.L., W.L., M.P.M., R.A.M., S.A.I.M., R.P.M., S.N., N.E.O., K.S., M.S., S.S., H.A.T., N.E.W.; investigation, L.P.W., J.V.M., R.M.C., B.F.R., W.V.Z., Q.A., Y.A., W.R.B., R.F.B., R.G.B., T.J.B., D.L.B., J.H.B., N.W.C., S.C., P.F.D., M.H.I., M.K., J.F.K., A.W.L., W.L., L.L., M.P.M., R.A.M., J.G.M., J.W.M., S.A.I.M., R.P.M., S.N., M.A.O., N.E.O., I.M.P., K.S., M.S., S.S., H.A.T., N.E.W., J.E.W., D.W., A.T.W.; resources, J.V.M., R.M.C., B.F.R., W.R.B., J.H.B., N.W.C., S.C., J.F.K., L.L., R.A.M., J.G.M., J.W.M., S.A.I.M., G.A.d.N., S.N., S.S.; data curation, W.V.Z., N.W.C., J.F.K., M.A.O.; writing—original draft preparation, B.F.R., W.V.Z.; writing—review and editing, L.P.W., J.V.M., R.M.C., B.F.R., Q.A., Y.A., W.R.B., R.F.B., R.G.B., T.J.B., D.L.B., J.H.B., N.W.C., S.C., P.F.D., M.H.I., M.K., J.F.K., A.W.L., W.L., L.L., M.P.M., R.A.M., J.G.M., J.W.M., S.A.I.M., R.P.M., G.A.d.N., S.N., M.A.O., N.E.O., I.M.P., K.S., M.S., S.S., H.A.T., N.E.W., J.E.W., D.W., A.T.W.; visualization, L.P.W., B.F.R., W.V.Z., Y.A., W.R.B., D.L.B., N.W.C., S.C., J.F.K., W.L., M.P.M., S.A.I.M., R.P.M., S.N., N.E.O., K.S., M.S., H.A.T., N.E.W., J.E.W., D.W.; supervision, J.V.M., B.F.R., W.V.Z., W.R.B., R.F.B., R.G.B., T.J.B., J.H.B., N.W.C., S.C., P.F.D., M.H.I., M.K., J.F.K., L.L., R.A.M., J.W.M., R.P.M., G.A.d.N., S.N., M.S., S.S., N.E.W., J.E.W.; project administration, B.F.R., W.V.Z., W.R.B., N.W.C., S.C., J.F.K., L.L., R.A.M., J.W.M., G.A.d.N., S.N., M.S., S.S., J.E.W.; funding acquisition, J.V.M., B.F.R., W.V.Z., W.R.B., R.G.B., T.J.B., N.W.C., S.C., P.F.D., M.H.I., J.F.K., R.A.M., J.W.M., G.A.d.N., S.N., M.S., N.E.W. All authors have read and agreed to the published version of the manuscript.

Funding: SuperTIGER has been funded by NASA under grant numbers NNX09AC17G, NNX14AB25G, NNX15AC23G, and 80NSSC20K0405. TIGERISS is funded by NASA under cooperative agreement number 80NSSC22M0299.

Data Availability Statement: No new data were created or analyzed in this study. Data sharing is not applicable to this article.

Acknowledgments: SuperTIGER was supported by Cecil J. Waddington at the University of Minnesota until he passed on October 1, 2020. SuperTIGER has also been supported by M. E. Wiedenbeck. SuperTIGER and TIGERISS efforts at Washington University in St. Louis have also been supported by the McDonnell Center for the Space Sciences and the Peggy and Steve Fossett Foundation.

Conflicts of Interest: The authors declare no conflicts of interest.

Abbreviations

The following abbreviations are used in this manuscript:

MDPI	Multidisciplinary Digital Publishing Institute
ACE	Advanced Composition Explorer
ADAPT	Antarctic Demonstrator for the Advanced Particle-astrophysics Telescope
AGILE	Light Imager for Gamma-ray Astrophysics
AMS	Alpha Magnetic Spectrometer
APT	Advanced Particle-astrophysics Telescope
BAS	Balloon Air Sampler
BNSM	binary neutron star merger
Caltech	California Institute of Technology
CALET	CALorimetric Electron Telescope
COVID-19	coronavirus disease 2019
CR	cosmic ray
CRIS	Cosmic Ray Isotope Spectrometer
DAMPE	Dark Matter Particle Explorer
DAQ	data acquisition
EAS	extensive air shower
ECOSTRESS	ECOSystem Spaceborne Thermal Radiometer Experiment on Space Station

EFU	Exposed Facility Unit
ELC	ExPRESS Logistics Carrier
E-MIST	Exposing Microorganisms in the Stratosphere
EPACT	Energetic Particles: Acceleration, Composition, and Transport investigation
ESA	European Space Agency
ExPRESS	EXpedite the PROcessing of Experiments to the Space Station
FPGA	field-programmable gate array
GCR	galactic cosmic rays
GEDI	Global Ecosystem Dynamics Investigation
GGG	Global Geospace Science
HARP	HyperAngular Rainbow Polarimeter
HEAO	High-Energy Astronomy Observatory
HELIX	High-Energy Light Isotope eXperiment
HNE	Heavy Nuclei Experiment
INCA	Ionospheric Neutron Content Analyzer
ISM	interstellar media
ISS	International Space Station
JAXA	Japan Aerospace Exploration Agency
JEM	Japanese Experiment Module
LAT	Large-Area Telescope
LDB	Long-Duration Balloon
LDEF	Long-Duration Exposure Facility
NASA	National Aeronautics and Space Administration
NKU	Northern Kentucky University
NSM	Neutron Star Merger
PACE	Plankton, Aerosol, Clouds, ocean Ecosystem
PAMELA	Payload for Antimatter Matter Exploration and Light-nuclei Astrophysics
PMC-Turbo	Polar Mesospheric Cloud Turbulence
PMT	photomultiplier tube
PSU	Pennsylvania State University
SiPM	silicon photomultiplier
SN	supernova
SNe	supernovae
SONTRAC	Solar Neutron TRACKing
SOX	Starboard Overhead X-Direction
SS	Solar System
SSD	silicon strip detector
STEREO	Solar Terrestrial Relations Observatory
SuperTIGER	Super Trans-Iron Galactic Element Recorder
TIGER	Trans-Iron Galactic Element Recorder
TIGERISS	Trans-Iron Galactic Element Recorder for the International Space Station
TRL	Technology Readiness Level
UHCRE	Ultra-Heavy Cosmic Ray Experiment
UHECR	ultra-high energy cosmic ray
UHGCR	ultra-heavy galactic cosmic ray
UMBC	University of Maryland Baltimore County
WUSTL	Washington University in St. Louis

References

1. Walsh, N.E. SuperTIGER Elemental Abundances for the Charge Range $41 \leq Z \leq 56$. Ph.D. Thesis, Washington University, St. Louis, MI, USA, 2020.
2. Walsh, N.E.; Akaike, Y.; Binns, W.; Bose, R.; Brandt, T.; Braun, D.; Cannady, N.; Dowkontt, P.; Hams, T.; Israel, M.; et al. SuperTIGER Abundances of Galactic Cosmic Rays for the Atomic Number (Z) Interval 30 to 56. In Proceedings of the 37th International Cosmic Ray Conference (ICRC2021), Berlin, Germany, 12–23 July 2021; Volume 395. [\[CrossRef\]](#)
3. Walsh, N.E.; Akaike, Y.; Binns, W.R.; Bose, R.G.; Brandt, T.J.; Braun, D.L.; Cannady, N.W.; Dowkontt, P.F.; Hams, T.; Israel, M.H.; et al. SuperTIGER instrument abundances of galactic cosmic rays for the charge interval $41 \leq Z \leq 56$. *Adv. Space Res.* **2022**, *70*, 2666–2673. [\[CrossRef\]](#)

4. Walsh, N.E. SuperTIGER Abundances of Galactic Cosmic Rays for the Atomic Number (Z) Interval 40 to 56. In Proceedings of the 38th International Cosmic Ray Conference (ICRC2023), Nagoya, Japan, 26 July–3 August 2023; Volume 444, p. 053. [[CrossRef](#)]
5. Rauch, B.F.; Zober, W.V.; Borda, R.F.; Bose, R.G.; Braun, D.L.; Buckley, J.; Calderon, J.; Cannady, N.W.; Caputo, R.; Coutu, S.; et al. The Trans-Iron Galactic Element Recorder for the International Space Station (TIGERISS). In Proceedings of the 38th International Cosmic Ray Conference (ICRC2023), Nagoya, Japan, 26 July–3 August 2023; Volume 444, p. 171. [[CrossRef](#)]
6. Rauch, B.F.; Zober, W.V.; Borda, R.F.; Bose, R.G.; Braun, D.L.; Buckley, J.; Calderon, J.; Cannady, N.W.; Caputo, R.; Coutu, S.; et al. Modeling Expected TIGERISS Observations. In Proceedings of the 38th International Cosmic Ray Conference (ICRC2023), Nagoya, Japan, 26 July–3 August 2023; Volume 444, p. 172. [[CrossRef](#)]
7. Abbott, B.P.; Abbott, R.; Abbott, T.D.; Acernese, F.; Ackley, K.; Adams, C.; Adams, T.; Addesso, P.; Adhikari, R.X.; Adya, V.B.; et al. GW170817: Observation of Gravitational Waves from a Binary Neutron Star Inspiral. *Phys. Rev. Lett.* **2017**, *119*, 161101. [[CrossRef](#)] [[PubMed](#)]
8. Abbott, B.P.; Abbott, R.; Abbott, T.D.; Acernese, F.; Ackley, K.; Adams, C.; Adams, T.; Addesso, P.; Adhikari, R.X.; Adya, V.B.; et al. Multi-messenger Observations of a Binary Neutron Star Merger. *Astrophys. J. Lett.* **2017**, *848*, L12. [[CrossRef](#)]
9. Zober, W.V.; Rauch, B.F.; Borda, R.F.; Bose, R.G.; Braun, D.L.; Buckley, J.; Calderon, J.; Cannady, N.W.; Caputo, R.; Coutu, S.; et al. Science Objectives and Goals of the TIGERISS mission. In Proceedings of the 38th International Cosmic Ray Conference (ICRC2023), Nagoya, Japan, 26 July–3 August 2023; Volume 444, p. 144. [[CrossRef](#)]
10. Marrocchesi, P. CALET: A calorimeter-based orbital observatory for High Energy Astroparticle Physics. *Nucl. Instrum. Methods Phys. Res. Sect. A* **2012**, *692*, 240–245. [[CrossRef](#)]
11. Sun, H.; Alemanno, F.; Altomare, C.; An, Q.; Azzarello, P.; Barbato, F.C.T.; Bernardini, P.; Bi, X.J.; Cagnoli, I.; Cai, M.S.; et al. Measurement of Heavy Nuclei beyond Iron in Cosmic Rays with the DAMPE Experiment. In Proceedings of the 38th International Cosmic Ray Conference (ICRC2023), Nagoya, Japan, 26 July–3 August 2023; Volume 444, p. 174. [[CrossRef](#)]
12. Israel, M.H.; Lave, K.A.; Wiedenbeck, M.E.; Binns, W.R.; Christian, E.R.; Cummings, A.C.; Davis, A.J.; de Nolfo, G.A.; Leske, R.A.; Mewaldt, R.A.; et al. Elemental Composition at the Cosmic-Ray Source Derived from the ACE-CRIS Instrument. I. ${}^6\text{C}$ to ${}^{28}\text{Ni}$. *Astrophys. J.* **2018**, *865*, 69. [[CrossRef](#)]
13. Binns, W.R.; Wiedenbeck, M.E.; von Rosenvinge, T.T.; Israel, M.H.; Christian, E.R.; Cummings, A.C.; de Nolfo, G.A.; Leske, R.A.; Mewaldt, R.A.; Stone, E.C. The Isotopic Abundances of Galactic Cosmic Rays with Atomic Number $29 \leq Z \leq 38$. *Astrophys. J.* **2022**, *936*, 13. [[CrossRef](#)]
14. Binns, W.R.; Garrard, T.L.; Gibner, P.S.; Israel, M.H.; Kertzman, M.P.; Klarmann, J.; Newport, B.J.; Stone, E.C.; Waddington, C.J. Abundances of Ultraheavy Elements in the Cosmic Radiation: Results from HEAO 3. *Astrophys. J.* **1989**, *346*, 997. [[CrossRef](#)]
15. Fowler, P.H.; Walker, R.N.F.; Mashedier, M.R.W.; Moses, R.T.; Worley, A.; Gay, A.M. Ariel 6 Measurements of the Fluxes of Ultra-heavy Cosmic Rays. *Astrophys. J.* **1987**, *314*, 739. [[CrossRef](#)]
16. Price, P.B.; Lowder, D.M.; Westphal, A.J.; Wilkes, R.D.; Brennen, R.A.; Afanasiev, V.G.; Akimov, V.V.; Rodin, V.G.; Baryshnikov, G.K.; Gorshkov, L.A.; et al. Trek-a Cosmic-Ray Experiment on the Russian Space Station MIR. *Astrophys. Space Sci.* **1992**, *197*, 121–143. [[CrossRef](#)]
17. Westphal, A.J.; Price, P.B.; Weaver, B.A.; Afanasiev, V.G. Evidence against stellar chromospheric origin of Galactic cosmic rays. *Nature* **1998**, *396*, 50–52. [[CrossRef](#)]
18. Donnelly, J.; Thompson, A.; O’Sullivan, D.; Daly, J.; Drury, L.; Domingo, V.; Wenzel, K.P. Actinide and Ultra-Heavy Abundances in the Local Galactic Cosmic Rays: An Analysis of the Results from the LDEF Ultra-Heavy Cosmic-Ray Experiment. *Astrophys. J.* **2012**, *747*, 40. [[CrossRef](#)]
19. Murphy, R.P. Identifying the Origin of Galactic Cosmic Rays with the SuperTIGER Instrument. Ph.D. Thesis, Washington University, St. Louis, MI, USA, 2015.
20. Murphy, R.P.; Sasaki, M.; Binns, W.R.; Brandt, T.J.; Hams, T.; Israel, M.H.; Labrador, A.W.; Link, J.T.; Mewaldt, R.A.; Mitchell, J.W.; et al. Galactic Cosmic Ray Origins and OB Associations: Evidence from SuperTIGER Observations of Elements ${}^{26}\text{Fe}$ through ${}^{40}\text{Zr}$. *Astrophys. J.* **2016**, *831*, 148. [[CrossRef](#)]
21. Rauch, B.F.; Walsh, N.E.; Zober, W.V. SuperTIGER Ultra-Heavy Galactic Cosmic Ray Atmospheric Propagation Corrections and Uncertainty Analysis. In Proceedings of the 37th International Cosmic Ray Conference (ICRC2021), Berlin, Germany, 12–23 July 2021; Volume 395, p. 089. [[CrossRef](#)]
22. Rauch, B.F.; Bose, R.G.; West, A.T.; Lisalda, L.; Abarr, Q.; Akaike, Y.; Binns, W.; Brandt, T.; Braun, D.L.; Dowkontt, P.; et al. SuperTIGER-2 2018 Flight Payload Recovery and Preliminary Instrument Assessment. In Proceedings of the 36th International Cosmic Ray Conference (ICRC2019), Madison, WI, USA, 24 July–1 August 2019; Volume 358, p. 131. [[CrossRef](#)]
23. Link, J.T. Measurements of Ultra-Heavy Galactic Cosmic Rays with the TIGER Instrument. Ph.D. Thesis, Washington University, St. Louis, MI, USA, 2003.
24. Link, J.T.; Barbier, L.M.; Binns, W.R.; Christian, E.R.; Cummings, J.R.; de Nolfo, G.A.; Geier, S.; Israel, M.H.; Mewaldt, R.A.; Mitchell, J.W.; et al. Measurements of the Ultra-Heavy Galactic Cosmic-Ray Abundances between $Z = 30$ and $Z = 40$ with the TIGER Instrument. In Proceedings of the 28th International Cosmic Ray Conference, Tsukuba, Japan, 31 July–7 August 2003.
25. Rauch, B.F. Measurement of the Relative Abundances of the Ultra-Heavy Galactic Cosmic Rays ($30 \leq Z \leq 40$) with the Trans-Iron Galactic Element Recorder (TIGER) Instrument. Ph.D. Thesis, Washington University, St. Louis, MI, USA, 2008.

26. Rauch, B.F.; Link, J.T.; Lodders, K.; Israel, M.H.; Barbier, L.M.; Binns, W.R.; Christian, E.R.; Cummings, J.R.; de Nolfo, G.A.; Geier, S.; et al. Cosmic Ray origin in OB Associations and Preferential Acceleration of Refractory Elements: Evidence from Abundances of Elements ^{26}Fe through ^{34}Se . *Astrophys. J.* **2009**, *697*, 2083–2088. [[CrossRef](#)]
27. Lawrence, D.J. The trans-iron galactic element recorder: A detector that will measure the elemental abundances of the ultra-heavy cosmic rays. Ph.D. Thesis, Washington University, Saint Louis, MI, USA, 1996.
28. Sposato, S.H. The 1997 balloon flight of the trans-iron galactic element recorder. Ph.D. Thesis, Washington University, St. Louis, MI, USA, 1999.
29. Lawrence, D.J.; Barbier, L.M.; Beatty, J.J.; Binns, W.R.; Christian, E.R.; Crary, D.J.; Ficenc, D.J.; Hink, P.L.; Klarmann, J.; Krombel, K.E.; et al. Large-area scintillating-fiber time-of-flight/hodoscope detectors for particle astrophysics experiments. *Nucl. Instrum. Methods Phys. Res. A* **1999**, *420*, 402–415. [[CrossRef](#)]
30. Hughes, Z.; Buckley, J.; Bergström, L.; Binns, W.; Buhler, J.; Chen, W.; Cherry, M.; Funk, S.; Hooper, D.; Mitchell, J.; et al. Report of 2019 APTlite balloon flight. In Proceedings of the 236th American Astronomical Society Meeting, online, 1–3 June 2020; Volume 236, p. 142.04.
31. Hughes, Z.D. Toward an Understanding of High-Mass Gamma-Ray Binaries: An Investigation Using Current Observatories and the Development of a Future GeV Instrument. Ph.D. Thesis, Washington University, St. Louis, MI, USA, 2021.
32. Meshik, A.; Kehm, K.; Pravdivtseva, O.; Rauch, B. Measurements of Atmospheric Noble Gases in Antarctica Captured by Autonomous Balloon Sampling. In Proceedings of the AGU Fall Meeting Abstracts, Chicago, IL, USA, 12–16 December 2022; Volume 2022, pp. P54A–02.
33. Smith, D.J.; Thakrar, P.J.; Bharrat, A.E.; Dokos, A.G.; Kinney, T.L.; James, L.M.; Lane, M.A.; Khodadad, C.L.; Maguire, F.; Maloney, P.R.; et al. A Balloon-Based Payload for Exposing Microorganisms in the Stratosphere (E-MIST). *Gravit. Space Res.* **2022**, *2*, 70–80. [[CrossRef](#)]
34. Williams, B.P.; Kjellstrand, B.; Jones, G.; Reimuller, J.D.; Fritts, D.C.; Miller, A.; Geach, C.; Limon, M.; Hanany, S.; Kaifler, B.; et al. The PMC-Turbo Balloon Mission to Study Gravity Waves and Turbulence through High-Resolution Imaging of Polar Mesospheric Clouds. In Proceedings of the AGU Fall Meeting Abstracts, New Orleans, LA, USA, 11–15 December 2017; Volume 2017, pp. SA24A–08.
35. Binns, W.R.; Bose, R.G.; Braun, D.L.; Brandt, T.J.; Daniels, W.M.; Dowkontt, P.F.; Fitzsimmons, S.P.; Hahne, D.J.; Hams, T.; Israel, M.H.; et al. The SUPERTIGER Instrument: Measurement of Elemental Abundances of Ultra-Heavy Galactic Cosmic Rays. *Astrophys. J.* **2014**, *788*, 18. [[CrossRef](#)]
36. Sanuki, T.; Motoki, M.; Matsumoto, H.; Seo, E.S.; Wang, J.Z.; Abe, K.; Anraku, K.; Asaoka, Y.; Fujikawa, M.; Imori, M.; et al. Precise Measurement of Cosmic-Ray Proton and Helium Spectra with the BESS Spectrometer. *Astrophys. J.* **2000**, *545*, 1135–1142. [[CrossRef](#)]
37. Aguilar, M.; Alcaraz, J.; Allaby, J.; Alpat, B.; Ambrosi, G.; Anderhub, H.; Ao, L.; Arefiev, A.; Arruda, L.; Azzarello, P.; et al. Isotopic Composition of Light Nuclei in Cosmic Rays: Results from AMS-01. *Astrophys. J.* **2011**, *736*, 105. [[CrossRef](#)]
38. Engelmann, J.J.; Ferrando, P.; Soutoul, A.; Goret, P.; Juliussen, E.; Koch-Miramond, L.; Lund, N.; Masse, P.; Peters, B.; Petrou, N.; et al. Charge composition and energy spectra of cosmic-ray nuclei for elements from Be to Ni - Results from HEAO-3-C2. *Astron. Astrophys.* **1990**, *233*, 96–111.
39. Lodders, K. Solar System Abundances and Condensation Temperatures of the Elements. *Astrophys. J.* **2003**, *591*, 1220–1247. [[CrossRef](#)]
40. Woosley, S.E.; Heger, A. Nucleosynthesis and remnants in massive stars of solar metallicity. *Phys. Rep.* **2007**, *442*, 269–283. [[CrossRef](#)]
41. Lingefelter, R.E. The Origin of Cosmic Rays: How Their Composition Defines Their Sources and Sites and the Processes of Their Mixing, Injection, and Acceleration. *Astrophys. J. Suppl. Ser.* **2019**, *245*, 30. [[CrossRef](#)]
42. Stone, E.C.; Cohen, C.M.S.; Cook, W.R.; Cummings, A.C.; Gauld, B.; Kecman, B.; Leske, R.A.; Mewaldt, R.A.; Thayer, M.R.; Dougherty, B.L.; et al. The Cosmic-Ray Isotope Spectrometer for the Advanced Composition Explorer. *Space Sci. Rev.* **1998**, *86*, 285–356. [[CrossRef](#)]
43. Prest, M.; Barbiellini, G.; Bordignon, G.; Fedel, G.; Liello, F.; Longo, F.; Pontoni, C.; Vallazza, E. The AGILE silicon tracker: An innovative γ -ray instrument for space. *Nucl. Instrum. Methods Phys. Res. A* **2003**, *501*, 280–287. [[CrossRef](#)]
44. Rapin, D.; AMS-Tracker Collaboration. The AMS-02 silicon tracker: First year on ISS in space. *Nucl. Instrum. Methods Phys. Res. A* **2013**, *718*, 524–526. [[CrossRef](#)]
45. von Rosenvinge, T.T.; Barbier, L.M.; Karsch, J.; Liberman, R.; Madden, M.P.; Nolan, T.; Reames, D.V.; Ryan, L.; Singh, S.; Trexel, H.; et al. The Energetic Particles: Acceleration, Composition, and Transport (EPACT) investigation on the WIND spacecraft. *Space Sci. Rev.* **1995**, *71*, 155–206. [[CrossRef](#)]
46. Atwood, W.B.; Abdo, A.A.; Ackermann, M.; Althouse, W.; Anderson, B.; Axelsson, M.; Baldini, L.; Ballet, J.; Band, D.L.; Barbiellini, G.; et al. The Large Area Telescope on the Fermi Gamma-Ray Space Telescope Mission. *Astrophys. J.* **2009**, *697*, 1071–1102. [[CrossRef](#)]
47. Straulino, S.; Adriani, O.; Bonechi, L.; Bongi, M.; Castellini, G.; D’Alessandro, R.; Gabbanini, A.; Grandi, M.; Papini, P.; Ricciarini, S.; et al. The PAMELA silicon tracker. *Nucl. Instrum. Methods Phys. Res. A* **2004**, *530*, 168–172. [[CrossRef](#)]

48. Wiedenbeck, M.E.; Burnham, J.A.; Cohen, C.M.S.; Cook, W.R.; Crabill, R.M.; Cummings, A.C.; Davis, A.J.; Kecman, B.; Labrador, A.W.; Leske, R.A.; et al. Thin silicon solid-state detectors for energetic particle measurements-Development, characterization, and application on NASA's Parker Solar Probe mission. *Astron. Astrophys.* **2021**, *650*, A27. [[CrossRef](#)]
49. Mewaldt, R.A.; Cohen, C.M.S.; Cook, W.R.; Cummings, A.C.; Davis, A.J.; Geier, S.; Kecman, B.; Klemic, J.; Labrador, A.W.; Leske, R.A.; et al. The Low-Energy Telescope (LET) and SEP Central Electronics for the STEREO Mission. *Space Sci. Rev.* **2008**, *136*, 285–362. [[CrossRef](#)]
50. Mitchell, J.G.; Bruno, A. Performance Characteristics of the Ionospheric Neutron Content Analyzer (INCA). In Proceedings of the 36th International Cosmic Ray Conference (ICRC2019), Madison, WI, USA, 24 July–1 August 2019; Volume 36, p. 53. [[CrossRef](#)]
51. Perkins, J.S.; Brewer, I.; Briggs, M.S.; Bruno, A.; Burns, E.; Caputo, R.; Cenko, B.; Cucchiara, A.; De Nolfo, G.; Dumonthier, J.; et al. BurstCube: A CubeSat for gravitational wave counterparts. *Proc. SPIE* **2020**, *11444*, [[CrossRef](#)]
52. Buckley, J.; Alnussirat, S.; Altomare, C.; Bose, R.G.; Braun, D.L.; Buckley, J.H.; Buhler, J.; Burns, E.; Chamberlain, R.D.; Chen, W.; et al. The Advanced Particle-astrophysics Telescope (APT) Project Status. In Proceedings of the 37th International Cosmic Ray Conference (ICRC2021), Berlin, Germany, 12–23 July 2021; Volume 395, p. 655. [[CrossRef](#)]
53. de Nolfo, G.A.; Mitchell, J.G.; Suarez, G.; Ryan, J.M.; Bruno, A.; Dumonthier, J.; Legere, J.; Messner, R.; Tatoli, T.; Williams, L. Next-generation Solar Neutron TRACKing (SONTRAC) instrument. *Nucl. Instrum. Methods Phys. Res. A* **2023**, *1054*, 168352. [[CrossRef](#)]
54. Jeon, H. The Design and Status of the HELIX Ring Imaging Cherenkov Detector and Hodoscope Systems. In Proceedings of the 38th International Cosmic Ray Conference (ICRC2023), Nagoya, Japan, 26 July–3 August 2023; Volume 444, p. 121. [[CrossRef](#)]
55. Martins, J.V.; Fernandez-Borda, R.; McBride, B.; Remer, L.; Barbosa, H.M.J. The Harp Hype Ran Gular Imaging Polarimeter and the Need for Small Satellite Payloads with High Science Payoff for Earth Science Remote Sensing. In Proceedings of the 2018 IEEE International Geoscience and Remote Sensing Symposium (IGARSS 2018), Valencia, Spain, 22–27 July 2018; pp. 6304–6307. [[CrossRef](#)]
56. Remer, L.A.; Knobelspiesse, K.; Zhai, P.W.; Xu, F.; Kalashnikova, O.V.; Chowdhary, J.; Hasekamp, O.; Dubovik, O.; Wu, L.; Ahmad, Z.; et al. Retrieving Aerosol Characteristics From the PACE Mission, Part 2: Multi-Angle and Polarimetry. *Front. Environ. Sci.* **2019**, *7*. [[CrossRef](#)]
57. Hulley, G.; Hook, S.; Fisher, J.; Lee, C. ECOSTRESS, A NASA Earth-Ventures Instrument for studying links between the water cycle and plant health over the diurnal cycle. In Proceedings of the 2017 IEEE International Geoscience and Remote Sensing Symposium (IGARSS), Fort Worth, TX, USA, 23–28 July 2017; pp. 5494–5496. [[CrossRef](#)]
58. Dubayah, R.; Blair, J.B.; Goetz, S.; Fatoyinbo, L.; Hansen, M.; Healey, S.; Hofton, M.; Hurtt, G.; Kellner, J.; Luthcke, S.; et al. The Global Ecosystem Dynamics Investigation: High-resolution laser ranging of the Earth's forests and topography. *Sci. Remote Sens.* **2020**, *1*, 100002. [[CrossRef](#)]
59. B. F. Rauch for the CALET Collaboration. Predicted CALET measurements of ultra-heavy cosmic ray relative abundances. *Adv. Space Res.* **2014**, *53*, 1444–1450. [[CrossRef](#)]
60. George, J.S.; Lave, K.A.; Wiedenbeck, M.E.; Binns, W.R.; Cummings, A.C.; Davis, A.J.; de Nolfo, G.A.; Hink, P.L.; Israel, M.H.; Leske, R.A.; et al. Elemental Composition and Energy Spectra of Galactic Cosmic Rays During Solar Cycle 23. *Astrophys. J.* **2009**, *698*, 1666–1681. [[CrossRef](#)]
61. Rauch, B.F.; Walsh, N.E.; Zober, W.V. Determination of Expected TIGERISS Observations. In Proceedings of the 37th International Cosmic Ray Conference (ICRC2021), Berlin, Germany, 12–23 July 2021; Volume 395, p. 088. [[CrossRef](#)]

Disclaimer/Publisher's Note: The statements, opinions and data contained in all publications are solely those of the individual author(s) and contributor(s) and not of MDPI and/or the editor(s). MDPI and/or the editor(s) disclaim responsibility for any injury to people or property resulting from any ideas, methods, instructions or products referred to in the content.